Tunnelling and Underground Space Technology 49 (2015) 18–34

Contents lists available at ScienceDirect

Tunnelling and Underground Space Technology

journal homepage: www.elsevier.com/locate/tust

Three-dimensional face stability analysis of pressurized tunnels driven in a multilayered purely frictional medium

Eliane Ibrahim [a,*], Abdul-Hamid Soubra [a], Guilhem Mollon [b], Wassim Raphael [c], Daniel Dias [d], Ali Reda [e]

[a] University of Nantes, Saint-Nazaire, France
[b] LaMCoS, CNRS UMR 5259, INSA Lyon, Université de Lyon, France
[c] Civil and Environmental Engineering Department, Ecole Supérieure d'Ingénieurs de Beyrouth, USJ, Beirut, Lebanon
[d] Grenoble Alpes University, LTHE, F-38000 Grenoble, France
[e] Dar Al-Handasah (Shair and Partners), Lebanon

ARTICLE INFO

Article history:
Received 28 April 2014
Received in revised form 24 February 2015
Accepted 1 April 2015

Keywords:
Tunnel face stability
Upper-bound limit analysis method
Pressurized shield
Collapse
Multilayered frictional medium

ABSTRACT

This paper aims at presenting a three-dimensional (3D) failure mechanism for a circular tunnel driven under a compressed air shield in the case of a dry multilayered purely frictional soil. This mechanism is an extension of the limit analysis rotational failure mechanism developed by Mollon et al. (2011a) in the case of a single frictional layer. The results of the present mechanism are compared (in terms of the critical collapse pressure and the corresponding shape of the collapse mechanism) with those of a numerical model based on Midas-GTS software. Both models were found to be in good agreement. Furthermore, the proposed mechanism has the significant advantage of reduced computation time when compared to the numerical model. Thus, it can be used in practice (for preliminary design studies) in the case of a multilayered soil medium.

1. Introduction

When dealing with tunnels driven by a pressurized shield, two major concerns are addressed, corresponding to both ultimate and service limit states. The first is to ensure face stability by applying a pressure to the tunnel face and thus avoid collapse. The second is to limit ground displacements that propagate to the surface and may have impact on existing structures in case the tolerable deformations thresholds are exceeded. These displacements, in the case of shield tunneling, are affected by the amount of applied face pressure, but they are mostly affected, as per Vanoudheusden (2006), by the shield tail void and to the construction process itself. Therefore, this paper will only focus on the first problem of computing the minimal pressure required to prevent the soil collapse at the tunnel face.

Experimental, analytical and numerical approaches have been developed to determine the critical face pressure. The experimental studies were conducted using small-scale laboratory centrifuge tests (Al-Hallak, 1999; Chambon and Corté, 1994; Takano et al., 2006). On the other hand, the analytical approaches were based on limit equilibrium methods (Anagnostou, 2012; Anagnostou and Kovari, 1994; Broere, 2001; Horn, 1961) or limit analysis methods (Leca and Dormieux, 1990; Mollon et al., 2009a, 2010, 2011a, 2011b, 2012, 2013b; Soubra, 2002; Subrin and Wong, 2002). As for the numerical approach, although computationally expensive, it is nowadays the most popular method due to the development of powerful numerical tools allowing for 3D analysis (Al-Hallak, 1999; Dias, 1999; Mollon et al., 2009b, 2011c, 2013a; Yoo and Shin, 2003).

While most of the developed analytical failure mechanisms target the face stability of tunnels driven in a homogeneous soil layer (considering either frictional or purely cohesive soil), this paper aims at developing a failure mechanism for a multilayered frictional medium. The case of circular tunnels of diameter D and a cover depth C (where $C/D > 1$) supported with a uniform face pressure is considered in the analysis. The applied uniform face pressure may be associated with an air pressurized shield. The present mechanism is based on the three-dimensional (3D) rotational failure mechanism developed by Mollon et al. (2011a) in the case of a single frictional layer. A comparison between the results of the present 3D failure mechanism (in terms of the critical collapse pressure and the corresponding shape of the collapse mechanism) and the ones obtained using the numerical software Midas-GTS is presented and discussed.

* Corresponding author. Tel.: +961 70 906380.
E-mail address: eliane.ibrahim@dargroup.com (E. Ibrahim).

http://dx.doi.org/10.1016/j.tust.2015.04.001
0886-7798/

2. Literature review

2.1. Existing experimental tests

Experimental tests have been performed in order to visualize the collapse pattern at the tunnel face and to determine the corresponding value of the critical face pressure (e.g. Ahmed and Iskander, 2012; Berthoz et al., 2012; Chambon and Corté, 1994; Chen et al., 2013; Idinger et al., 2011; Kirsch, 2010; Takano et al., 2006). Meguid et al. (2008) presented a review of numerous physical models that were used to study the excavation of tunnels in soft ground.

Based on centrifuge tests, Chambon and Corté (1994) stated that the failure soil mass was found to resemble to a chimney that outcrops in the case of shallow tunnels and it is limited to 1D above the tunnel for deep tunnels. Takano et al. (2006) have shown by using X-ray computed tomography scanner that the failure shape can be simulated with a combination of logarithmic spirals and elliptical shapes in both vertical and horizontal directions respectively. Kirsch (2010), further to his small-scale model tests at single gravity, emphasized on the effect of soil density on the failure zone: (i) within dense sand, the failure zone is clearly defined and it progressively develops to reach the ground surface and (ii) for loose sands, no discrete collapse mechanism can be identified and movements immediately reach the surface. Idinger et al. (2011) and Ahmed and Iskander (2012) carried out centrifuge model tests, at 50g and 1g respectively, for various cover-to-diameter (C/D) ratios. The measured face pressure at collapse was found to be in good agreement with results from centrifuge tests performed at various gravitational accelerations (50g, 100g and 130g) by Chambon and Corté (1994). Both authors highlighted the influence of the cover-to-diameter (C/D) ratio on the vertical extent of the failure shape. The failure mechanism was found to outcrop for a C/D less than 1.0 as suggested by Idinger et al. (2011) and for a C/D less than 2.0 as stated by Ahmed and Iskander (2012). The local failure observed in front of the tunnel face by Chambon and Corté (1994), Idinger et al. (2011) and Ahmed and Iskander (2012), was also observed recently by Chen et al. (2013) on large-scale model tests. This local failure tends to reach the surface with time (Berthoz et al., 2012). Finally, notice that Berthoz et al. (2012) have observed that frictional soils with cohesion (though very slight of 0.5 kPa) manifest a failure shape in the form of a torus of decreasing section.

For tunnels drilled in multilayered soils, the experimental tests are in short supply since it is only recently that Berthoz et al. (2012) addressed the case of tunnels within stratified ground. In fact, these authors carried out a series of experimental tests on the ENTPE single gravity reduced-scale earth pressure balance shield model to analyze collapse and blow-out failure mechanisms. Among these tests, two (MS2 and MS3 models with two and three layered soils respectively) were performed. The first base layers below the tunnel axis, for both models, were constituted of a self-stable frictional–cohesive soil and are overlaid with purely frictional soil layers. A third cohesive–frictional layer with a small cohesion (c = 0.5 kPa) is added above the tunnel crown in the case of MS3 soil model. The failure shape observed for MS2 model resembles to a chimney beginning at the upper part of the excavation chamber. However, the collapse mechanism observed for MS3 model is composed of an extrusion within the purely frictional layer (i.e. upper half of the tunnel face), followed by the failure of a block above the tunnel crown within the frictional–cohesive layer, that extends upwards to reach the ground surface. Although the results by Berthoz et al. (2012) are the only ones that involve the case of a stratified soil medium, these results are limited to particular cases where the failure of the soil can occur only in the upper half of the tunnel face and it does not involve the entire face of the tunnel.

2.2. Limit analysis and existing failure mechanisms

Limit analysis is a method that assesses the failure load of a soil mass by giving upper- and lower-bounds on the exact limit load using kinematic and static approaches respectively. The kinematic approach based on rigid block mechanisms (cf. Chen, 1975 among others) is very popular. The major advantage of this method lies in its simplicity especially when it comes to the number of required input parameters and the fast computation time, making it suitable for preliminary design studies as well as for reliability-based analysis and design that require a great number of calls of the deterministic model. The failure is assumed to occur either by translation or rotation of a rigid body along the failure surface. In order to respect the normality condition of the limit analysis theory, the angle between the failure surface and the velocity vector should be equal to the soil internal friction angle.

The kinematic theorem of the limit analysis theory states that equating the rate of external work done by the external forces to the internal rate of energy dissipation for any kinematically admissible failure mechanism gives an unsafe solution of the limit load. In other words, the failure load deduced from a kinematically admissible mechanism is higher than (or equal to) the exact one. Notice that in the present case where the tunnel face pressure resists failure, the computed limit pressure is actually smaller than the exact one.

As mentioned in the previous section, several experimental tests have been performed in order to visualize the collapse pattern at the tunnel face. The failure soil mass was found to develop following a chimney-like shape (e.g. Chambon and Corté, 1994) that outcrops in the case of shallow tunnels and it is limited to 1D above the tunnel for deep tunnels. Based on these observations, Leca and Dormieux (1990) and Subrin and Wong (2002) proposed 3D failure mechanisms. The failure mechanism developed by Leca and Dormieux (1990) is a two-block translational kinematically admissible failure mechanism that is entirely defined by only one angular parameter. It is composed of two truncated conical blocks with circular cross-sections and with opening angles equal to 2φ in order to respect the normality condition in limit analysis. On the other hand, the failure mechanism developed by Subrin and Wong (2002) is a rotational mechanism depending on two parameters, and it is delimited by two logarithmic spirals in the longitudinal plane and a circle in any rotating plane. More recently, Mollon et al. (2010, 2011a) worked on the improvement of the existing solutions by first proposing a translational multi-block mechanism consisting of n truncated rigid blocks and then a rotational mechanism delimited by two logarithmic spirals in the central vertical plane of the tunnel. The major improvement brought by these new mechanisms is that they involve the entire circular face of the tunnel contrarily to the former mechanisms that only involved an elliptical area inscribed to the circular face (the other parts of the face remaining at rest). This was made possible by generating "point by point" the three-dimensional failure surface using a spatial discretization technique that starts from the contour of the circular tunnel face.

2.3. Comparison between existing experimental and analytical/numerical results

Fig. 1a and b shows the comparisons made respectively by Chen et al. (2013) and Kirsch (2010) involving the normalized face pressures at collapse as obtained by their experimental tests and by the

existing theoretical models. Chen et al. (2013) suggested considering a little cohesion in the upper bound analytical model (i.e. $c = 0.5$ kPa, "which can be due to the not fully dried sand"). This results in obtaining a closer value of the critical face pressure to the experimental one. The results from the analytical model by Mollon et al. (2011a) are added to Fig. 1 and are found to be in good agreement with the experimental results. The difference between the analytical normalized critical face pressure values ($N_D = \sigma_c/\gamma D$) from Mollon et al. (2011a) and the experimental results of Chen et al. (2013), considering a $c = 0.5$ kPa, varies between 9.5% and 2.5%. Also, when compared with the average of the normalized critical face pressure values Kirsch (2010) obtained from his experiments, the difference is found to be ranging between 26% and 1.4%. One can also notice the close matching between the results by Mollon et al. (2011a) and the numerical results by Vermeer et al. (2002). Similarly, the predictions of the stability condition of the tunnel face by Mollon et al. (2011a)'s theoretical model are consistent with the observations of Berthoz et al. (2012) experimental tests (see Table 2). For a soil with cohesion greater than or equal to 1.5 kPa the tunnel face is stable, while for cohesion of 0.5 kPa, the tunnel face is at the limit of failure.

Fig. 2a and b shows a comparison between the experimental failure shape given respectively by Kirsch (2010) and Berthoz (2012) and the theoretical failure mechanism obtained from Mollon et al. (2011a)'s theoretical model. A good agreement is

Table 1
Numerical model soil parameters.

Parameter		Unit	Soil layer 1	Soil layer 2
Soil Young modulus	E	(MPa)	75	75
Poisson's ratio	ν	(–)	0.22	0.22
Cohesion	c	(kPa)	0	0
Angle of internal friction	φ	(°)	45	30
Dilatancy angle	ψ	(°)	45	30
Soil unit weight	γ	(kN/m^3)	18	18
Earth pressure coefficient at rest	K_0	(–)	0.29	0.5

Table 2
Comparison between Berthoz et al. (2012) experimental observations and Mollon et al. (2011a) theoretical predictions.

Test No.	Parameters			Experimental observation	Theoretical prediction Mollon et al. (2011a)	
	c (kPa)	φ (°)	γ (kN/m^3)	Face stable without face pressure?	σ_c (kPa)	Face theoretically stable without face pressure?
MC2	2.5	36	13.2	Yes	−2.59	Yes
MC3	2.5	36	13.2	Yes	−2.59	Yes
MC4	1.5	36	13.2	Yes	−1.28	Yes
MC5	0.5	36	13.15	Yes	0.044	Critical stability
MC7	0.5	36	13.05	Yes	0.036	Critical stability
MC8	0.5	36	13.05	No	0.036	Critical stability

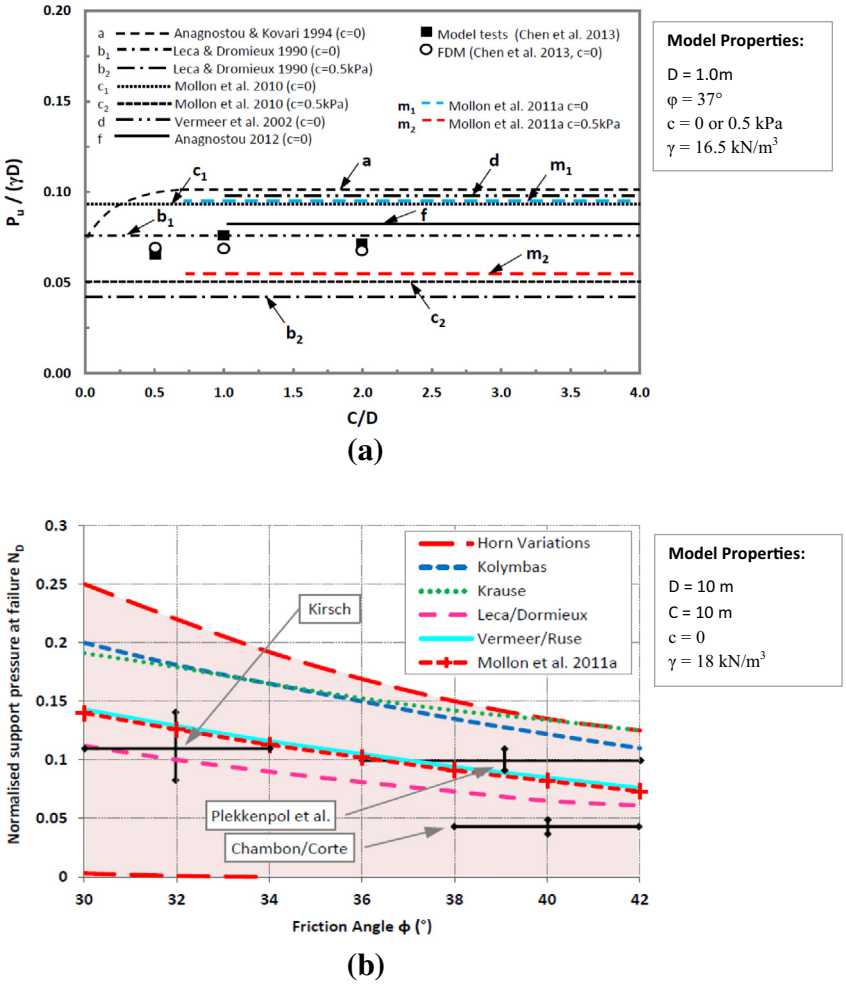

Fig. 1. Comparison of the normalized support pressure at failure $N_D = \sigma_c/\gamma D$ from different analytical failure mechanisms with the results from experimental tests (a) by Chen et al. (2013); (b) by Kirsch (2010).

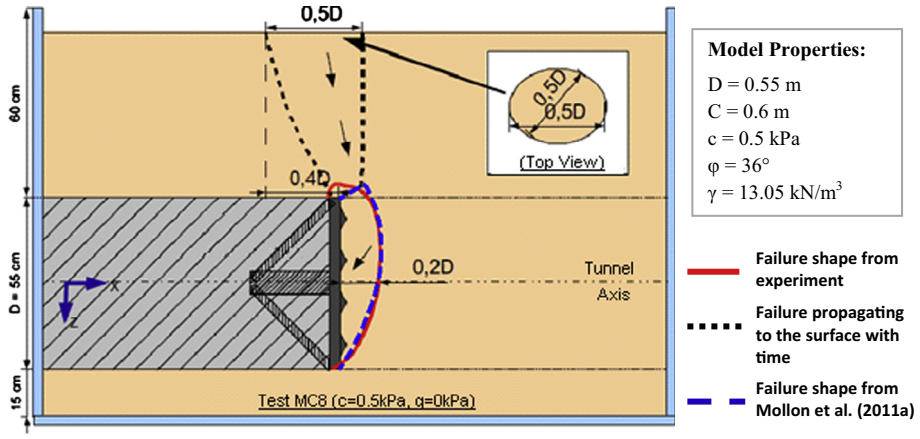

(a)

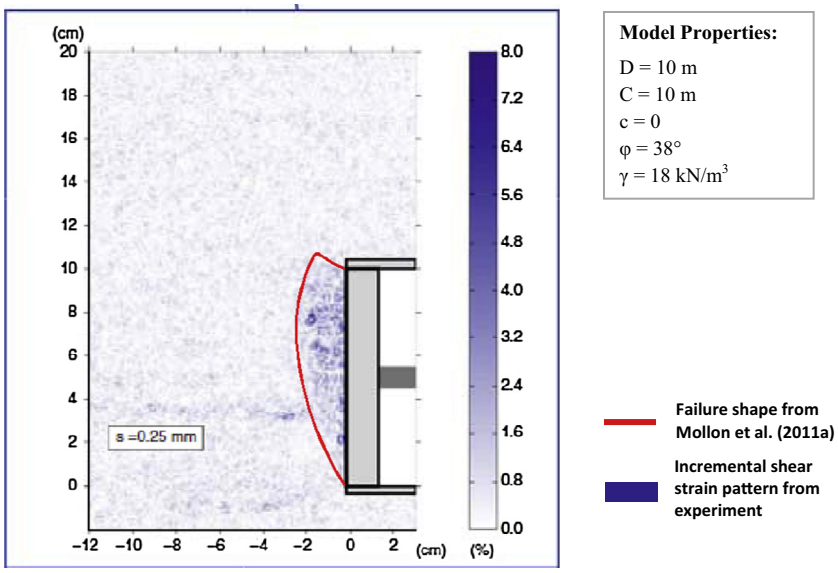

(b)

Fig. 2. Comparison of failure shape obtained from the analytical model by Mollon et al. (2011a) with the shape from experimental tests (a) by Berthoz (2012); (b) by Kirsch (2010).

observed between the experimental results and the results provided by Mollon et al. (2011a). However, failure might propagate with time to reach the surface as may be easily seen from the experimental results by Berthoz (2012) which are shown in Fig. 2(a). Notice finally that the failure shape obtained by Vermeer et al. (2002) was found to be in compliance with the experimental observations of Kirsch (2010) and Chen et al. (2013): for a friction angle of 20°, a chimney-like collapse mechanism is obtained, whereas for higher friction angles, "a relatively small body is dropping into the tunnel".

As a conclusion, the present section allows one to confirm that the 3D failure mechanism by Mollon et al. (2011a) gives accurate estimation of the collapse pressure and the corresponding shape of failure. Thus, in the following section, this mechanism is extended to the general case of a multilayered soil medium.

3. Limit analysis model for a multilayered frictional medium

Most of the aforementioned 3D mechanisms are developed for a one layer frictional soil. However, the encountered cases in practice are far from dealing with only one soil layer. Therefore, this paper proposes an extension of the 3D failure mechanism by Mollon et al. (2011a) to the case of a multilayered frictional medium. In this paper, the cover to diameter ratio C/D is taken equal to or higher than one to make sure that the failure is not affected by the overburden height and that the failure mechanism does not outcrop at the surface.

The rotational rigid block failure mechanism by Mollon et al. (2011a) has been proven to provide the best (highest) kinematical solution as compared to that obtained from the recent translational mechanism by Mollon et al. (2010) and all the previous kinematical approaches proposed by Leca and Dormieux, 1990; Subrin and Wong, 2002; Soubra, 2002; Mollon et al., 2009a, 2010. Furthermore, a good agreement was observed between this mechanism and the existing experimental results (see Section 2.3). Thus, the basic idea of this mechanism is used in this paper to develop a rotational mechanism for a multilayered frictional medium.

3.1. Construction of the 3D limit analysis model

The rotational failure mechanism undergoes a rotation about point O, with an angular velocity ω. At a given point of the

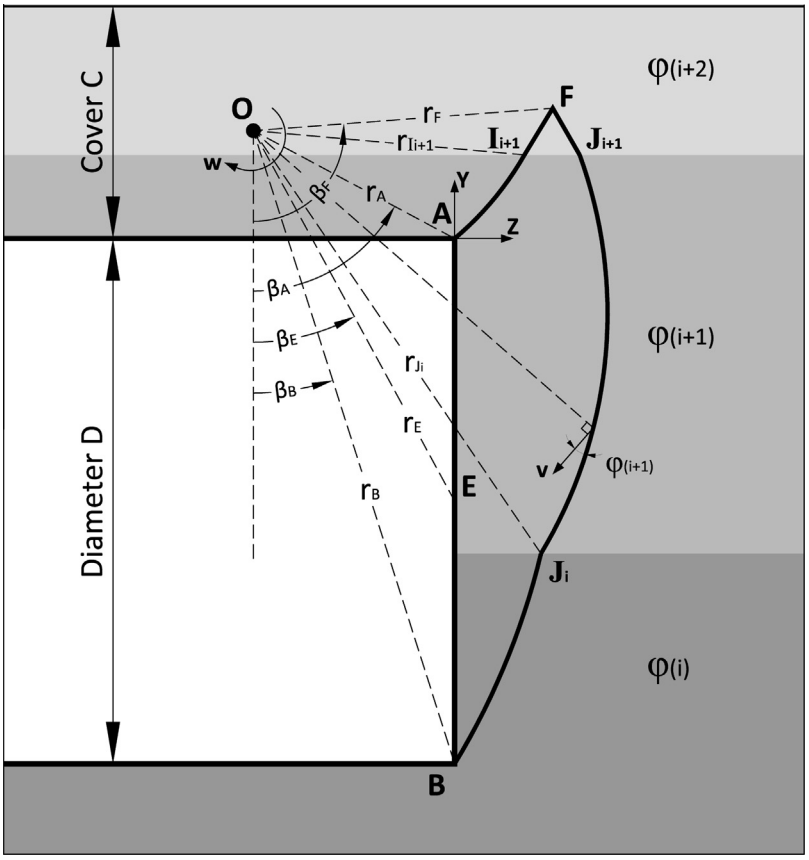

Fig. 3. Cross-section of the proposed failure mechanism in the (*Y*, *Z*) plane for a three-layers soil medium.

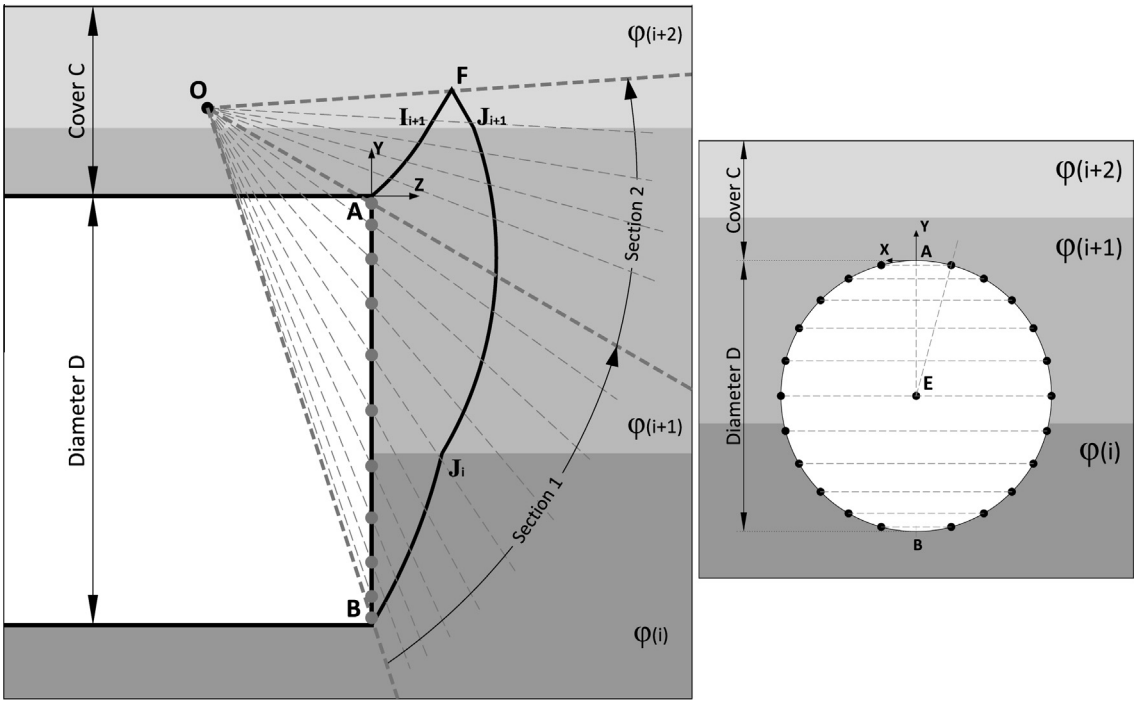

Fig. 4. Discretization technique for the generation of the proposed collapse mechanism.

mechanism, the norm of the velocity vector $\vec{v}$ is equal to $\omega \cdot r$ (r being the distance between that point and the center of rotation). The mechanism cross section in the central vertical plane of the tunnel is delimited by two logarithmic spirals of common center O emerging from the tunnel heading and invert and crossing the different soil layers (cf. Fig. 3). The angle between the velocity

vector and the failure surface is equal to φ_i where φ_i is the internal friction angle corresponding to the ith crossed soil layer. Hence, the normality condition of the kinematical approach is fully satisfied along the failure surface in the vertical central plane of the tunnel. Notice that although Fig. 3 is plotted for three layers denoted i, $i+1$ and $i+2$, the analysis for a greater number of layers is straightforward.

The method used to define the central vertical cross-section of the 3D mechanism is analogous to the one developed in a 2D spatially varying soil by Mollon et al. (2011b). In fact, two logarithmic spirals start at points A and B respectively, such as:

$$r = r_A \cdot \exp\left((\beta - \beta_A) \cdot \tan \varphi_{i+1}\right) \quad (1)$$

$$r = r_B \cdot \exp\left((\beta_B - \beta) \cdot \tan \varphi_i\right) \quad (2)$$

At each intersection point (I_i or J_i) between the logarithmic spirals and the horizontal line representing the top of the soil layer i (where points I_i involve the log-spiral emerging from A and points J_i are those involving the log-spiral emerging from B), a new logarithmic spiral is generated from this point using the friction angle corresponding to the new layer.

Let us assume that the failure mechanism does not outcrop and hence the defined slip lines meet at point F. The coordinates of point F can be deduced knowing that it belongs to two log-spirals emerging from the intersection points (I_{i+1} and J_{i+1}).

Having drawn the mechanism cross-section in the central vertical plane of the tunnel, the 3D failure surface is then generated by a "point by point" spatial discretization technique that makes use of the n radial planes (called hereafter construction planes) shown in Fig. 4. The contour of the tunnel face is first discretized by a

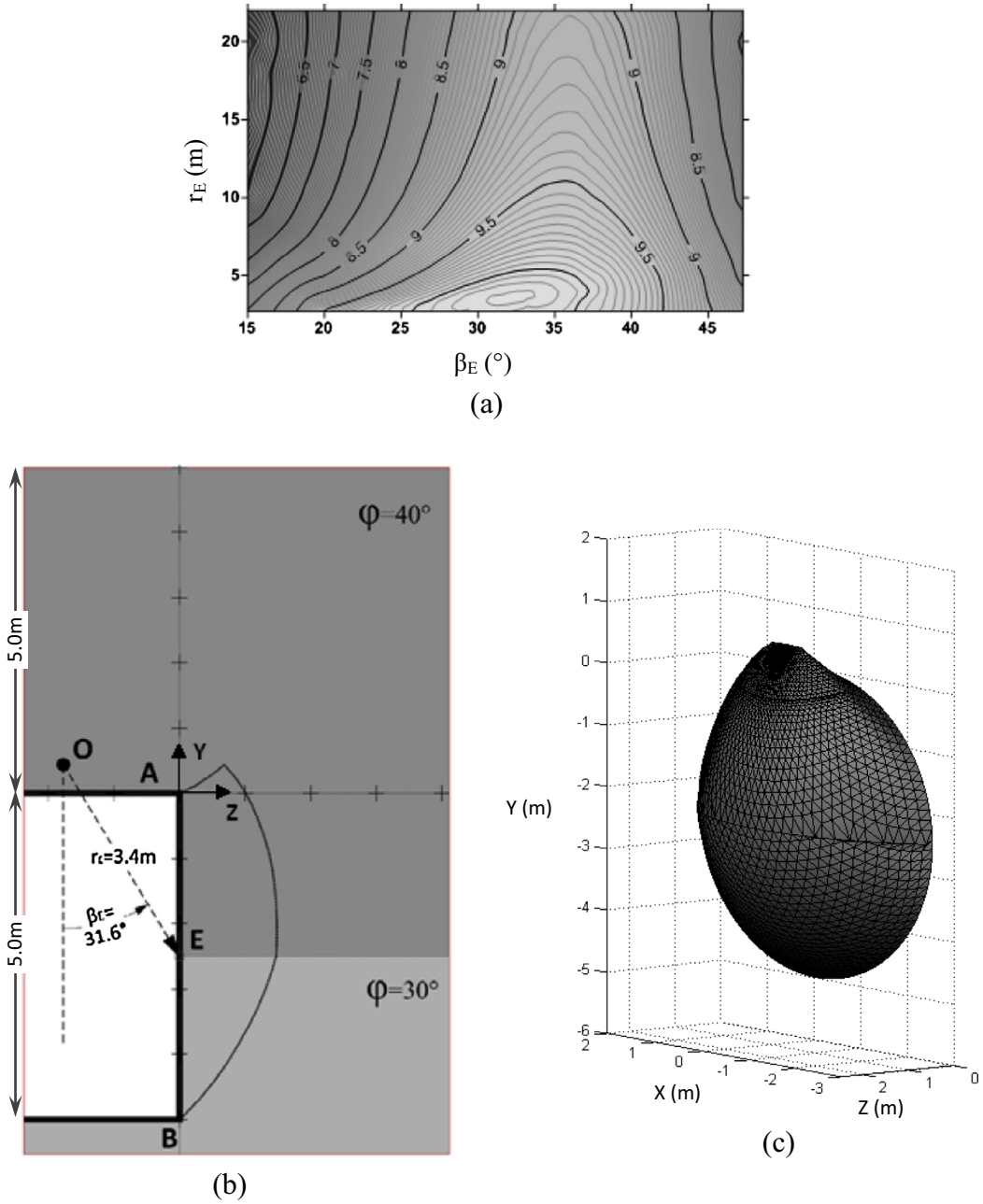

Fig. 5. Case of two frictional layers: (a) Response surface of the face pressure in the (β_E, r_E) plane where $\sigma_c = 10.1$ kPa (b) Critical failure mechanism in the central vertical plane where $\beta_E = 31.6°$ and $r_E = 3.40$ m and (c) 3D view of the critical failure mechanism.

number of points uniformly distributed and symmetrical with respect to the *Y* axis. A first set of radial planes is defined, each passing through 2 symmetrical points of the tunnel face. These planes cover the lower part of the mechanism (Section 1) comprised between the crest and the invert of the tunnel (points *A* and *B*), i.e. these planes 'cut' the tunnel face. A second set of radial planes (see Section 2) is then defined to cover the part of the mechanism between the tunnel crest and the tail of this mechanism (points *A* and *F*). In contrast to Section 1, the adjacent radial planes of Section 2 are assumed to be separated by a constant radial angle δ. Both sets of radial planes are defined by the index *j*.

Once the construction planes are defined, the mechanism will be built point by point. Departing from the points created on the contour of the tunnel face, new points will be created within the

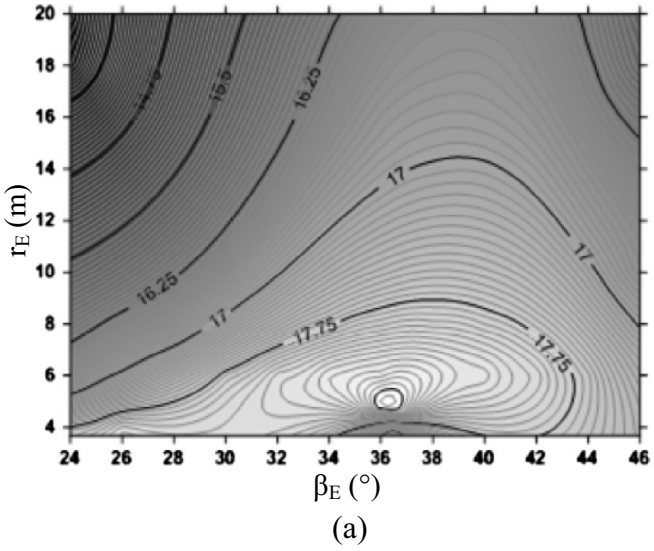

(a)

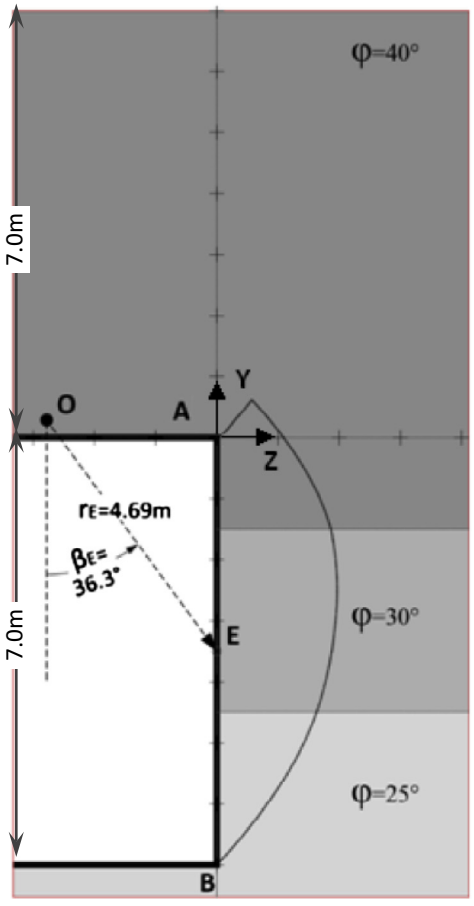

(b)

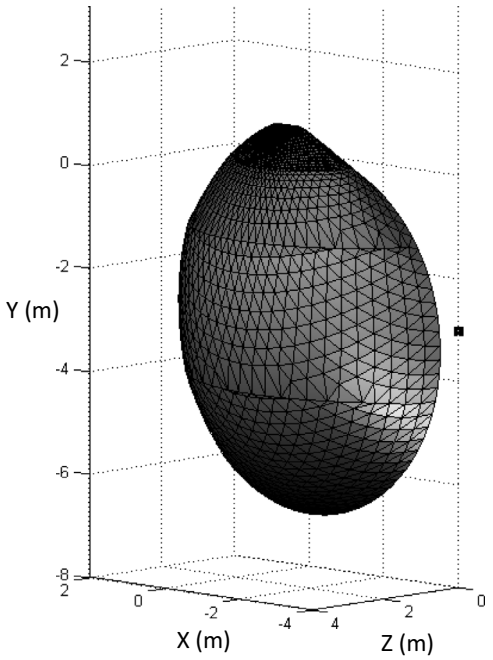

(c)

Fig. 6. Case of three frictional layers: (a) Response surface of the face pressure in the (β_E, r_E) plane where σ_c = 18.2 kPa (b) Critical failure mechanism in the central vertical plane where β_E = 36.3° and r_E = 4.69 m and (c) 3D view of the critical failure mechanism.

different already-defined radial planes (starting from the lower radial plane) and by respecting the normality condition, i.e. the angle between the velocity vector and the element of the failure surface (at any new point of the failure surface) should be equal to the internal friction angle φ_i of the enclosing soil layer. The external surface of the moving block is then defined by a collection of elementary triangular facets, $\Sigma_{k,j}$, linking the generated points, k representing the position of a given point on a given plane j. Subsequently, the volume of the rotating body is defined by elementary volumes, $V_{k,j}$, obtained from the projection of each of these facets on the central plane (Y, Z). When the mechanism has been generated up to the extremity F, one must check that it does not outcrop the ground surface. If so, then the part of the mechanism located above the ground surface is truncated and the intersection surface between the mechanism and the ground surface is computed by linear interpolation. For a more detailed description of the discretization and points generation techniques, reference should be made to Mollon et al. (2011a).

The determination of the collapse pressure is done by equating the rate of work of the external forces applied to the rigid rotating body to the rate of energy dissipation.

The external forces involved in the present mechanism are:

(i) The weight of the rigid block within layer i and having a unit weight γ_i, $(\dot{W}_\gamma)$;

$$\dot{W}_\gamma = \sum \left(\overrightarrow{\gamma_i} \cdot \overrightarrow{v_{kj}} \cdot V_{kj} \right) \tag{3}$$

(ii) A possible surcharge loading σ_s acting on the ground surface, $(\dot{W}_S)$. However, since it is assumed here that the mechanism does not outcrop, then:

$$\dot{W}_S = 0 \tag{4}$$

(iii) The collapse pressure σ of the tunnel face Σ', $(\dot{W}_\sigma)$;

$$\dot{W}_\sigma = \sum \left(\vec{\sigma} \cdot \overrightarrow{v_{kj}} \cdot \Sigma'_{i,j} \right) \tag{5}$$

The rate of work $(\dot{W})$ of each external force is found by summation of the elementary rates of works of all elementary surfaces (facets) and volumes created during the construction of the mechanism, taking into account the properties of each crossed layer.

As for the rate of internal energy dissipation $(\dot{W}_D)$ due to the soil plastic deformation, it is calculated along the envelope of the failure mechanism since the failure mechanism undergoes a rigid block movement. The rate of internal energy dissipation is $c_i \cdot \delta u$, where $\delta u = v \cdot \cos \varphi_i$ is the tangential component of the velocity along the velocity discontinuity surface and c_i the cohesion of the crossed layer i. Hence, at every intercepted new layer, the summation of the elementary energy dissipations along the elementary facets of the mechanism envelope within this layer is computed, taking into account the cohesion of the crossed layer.

$$\dot{W}_D = \sum \left(c_i \cdot v \cdot \cos \varphi_i \Sigma_{i,j} \right) \tag{6}$$

Finally, the work equation $\dot{W}_S + \dot{W}_\sigma + \dot{W}_\gamma = \dot{W}_D$ is simplified and written as follows:

$$\dot{W}_\sigma + \dot{W}_\gamma = 0 \tag{7}$$

The detailed description of the work equation within a single soil layer can be found in Mollon et al. (2011a). After simplifications made to the work equation, the tunnel collapse pressure is given by the following equation:

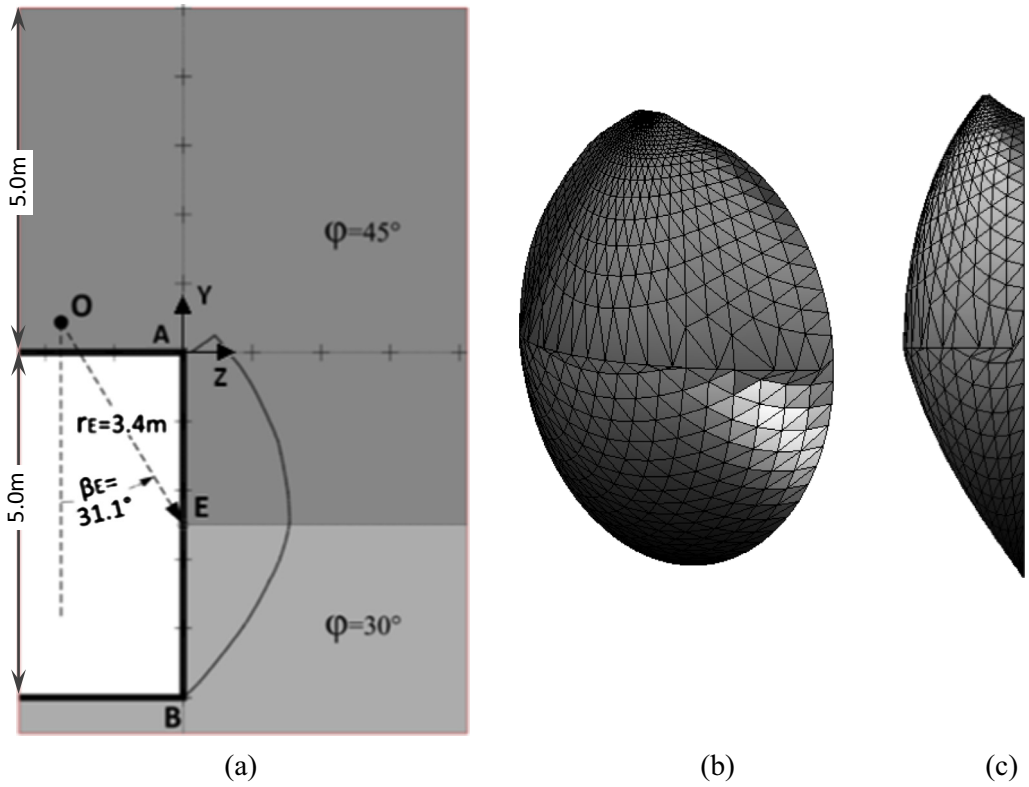

Fig. 7. Case of a tunnel driven in a two-layers frictional medium (a) cross-section of the critical failure mechanism (in the central vertical plane) as obtained from the analytical model (where $\sigma_c = 9.1$ kPa, $\beta_E = 31.1°$, $r_E = 3.4$ m) and (b and c) two 3D views of the mechanism.

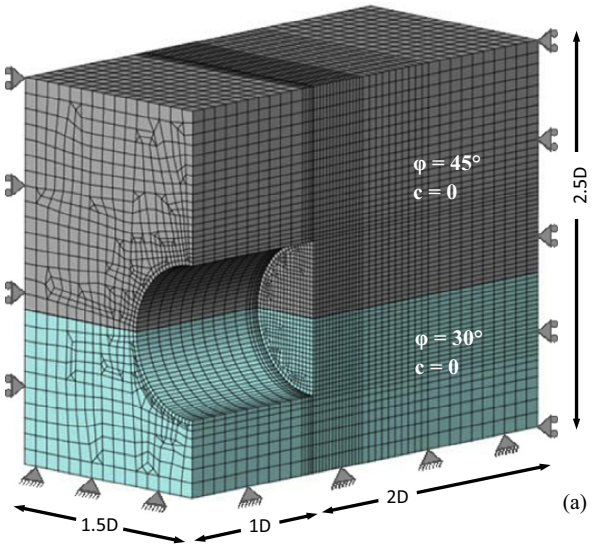

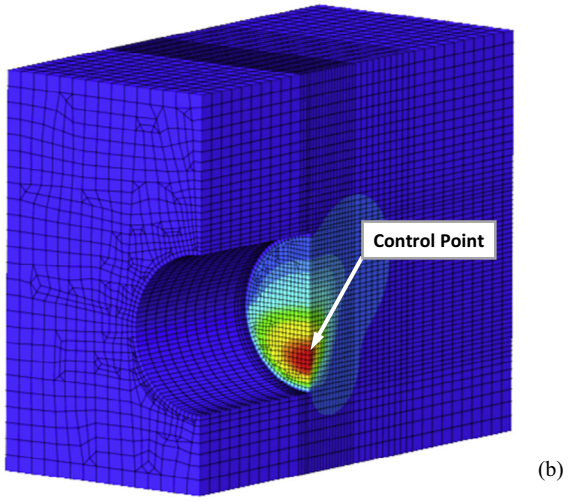

Fig. 8. Mesh used in the analysis (a) and maximum displacement control point for an applied face pressure of 10 kPa (b).

$$\sigma = D \cdot \frac{\sum \left(\overrightarrow{\gamma_i} \cdot \overrightarrow{v_{kj}} \cdot V_{kj} \right)}{D \cdot \sum \left(\vec{\sigma} \cdot \overrightarrow{v_{kj}} \cdot \Sigma'_{i,j} \right)} \tag{8}$$

In case a constant unit weight is adopted for all layers, as it is in this paper, Eq. (8) becomes

$$\sigma = \gamma \cdot D \cdot N_\gamma \tag{9}$$

where N_γ is a dimensionless coefficient, calculated along the different parts of the failure surface for the corresponding intercepted soil layer and representing the effect of soil weight.

It should be noted here, that in case $\dot{W}_D$ and $\dot{W}_S$ are not taken equal to zero, the tunnel collapse pressure will be given by the following more generic equation:

$$\sigma = D \cdot N_\gamma - N_c + \sigma_s \cdot N_s \tag{10}$$

If γ and c are assumed constant for all soil layers, then Eq. (10) becomes:

$$\sigma = \gamma \cdot D \cdot N_\gamma - c \cdot N_c + \sigma_s \cdot N_s \tag{11}$$

where N_c, and N_s are dimensionless coefficients similar to N_γ, calculated along the different parts of the failure surface for the corresponding intercepted soil layer, and representing the effect of cohesion and surcharge loading respectively.

It is important to note here that, in the case of multiple soil layers with different cohesion values, the proposed failure mechanism might not still applicable. This is due to the occurrence of localized failure zones that do not cover the whole tunnel face, similarly to what was observed by Berthoz et al. (2012). Therefore, it was decided to limit the proposed mechanism to the case of purely frictional soils and to soils with "slight" cohesion only.

The critical values of this coefficient can be obtained by maximization with respect to the two geometrical parameters r_E and β_E that describe the failure mechanism. As is well-known (cf. Soubra (1999) in the case of the bearing capacity of foundations), the optimization of these coefficients leads to an approximate but conservative estimation of the limit load. In this paper, the computation of the critical collapse pressure σ_c and the corresponding most critical failure mechanism is obtained rigorously by direct maximization of the tunnel pressure σ that is to say by minimization of $-\sigma$, knowing that the face pressure is a negative load that resists collapse, using the optimization algorithm tool implemented in Matlab software. This process uses an arbitrary user-defined set of parameters (r_E, β_E) in our case) as the starting point of the optimization and converges to the unique optimum by a sequence of computations of the tunnel face pressure at several points (r_E, β_E) of the space.

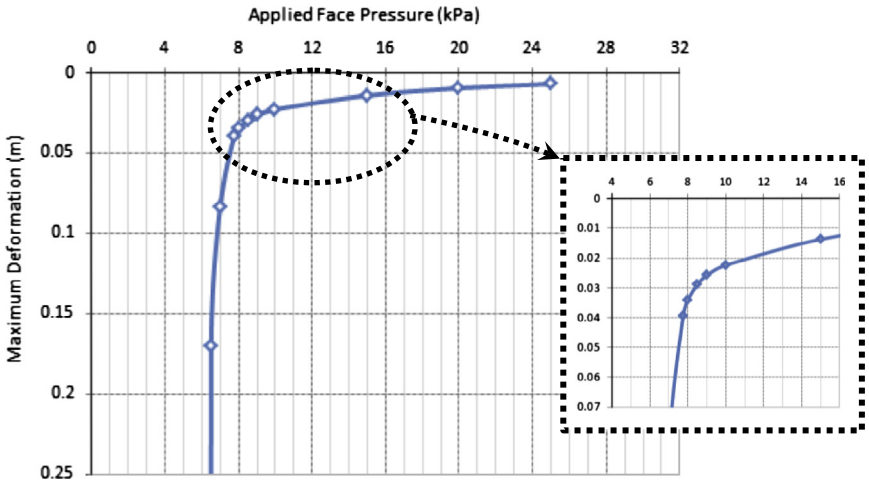

Fig. 9. Displacement versus applied face pressure as obtained by numerical simulation.

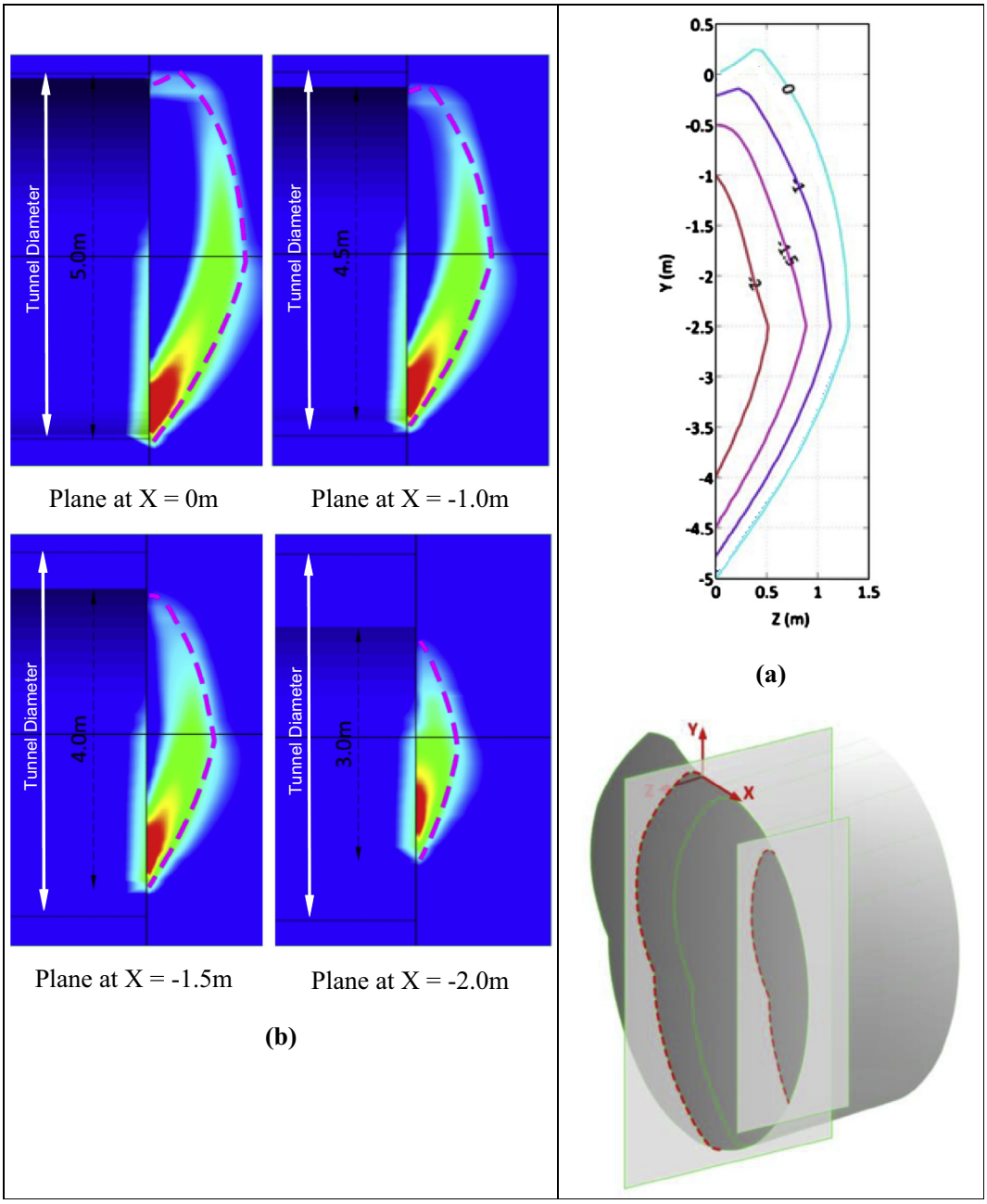

Fig. 10. Comparison between cross-sections through the 3D analytical and numerical models in the planes parallel to the (Y, Z) plane (at $X = 0$, -1.0, -1.5 and -2.0 m): (a) cross-sections through the 3D analytical failure mechanism (b) cross-sections through the 3D numerical model overlaid with the corresponding failure surface from the analytical model.

3.2. Uniqueness of the computed critical face pressure

For a one-layer frictional soil with a unique constant friction angle, one obtains a unique maximum soil pressure corresponding to the most critical failure mechanism. When it comes to the case of a heterogeneous soil, the 2D results presented in Mollon et al. (2011b) show that the possible presence of local maximums of the critical face pressure should be investigated. This issue is examined herein when considering a multilayered soil medium, using the response surface method. This method allows determining the relationship between the geometrical parameters (r_E and β_E) and the calculated response variable (i.e. the face pressure). Indeed; for a given tunnel model, the face pressure is calculated for a high number of generated mechanisms. The obtained values of the face pressure are plotted against the corresponding values of r_E and β_E. Contour lines are then drawn through equal values of the face pressure to check whether a unique or several maximums can be observed for the studied case.

In Figs. 5 and 6, the response surfaces are given for failure mechanisms generated in two and three soil layers, for tunnels diameters D of 5.0 m and 7.0 m respectively and for a 1D soil cover when the soil unit weight is equal to 18 kN/m^3. It can be clearly seen that no local maximums are observed: the contour lines converge toward a single maximum corresponding to the unique most critical failure mechanism for the given soil and geometric conditions. Therefore, the common optimization methods, such as those

implemented in Matlab (i.e. using "fminsearch" function), can be easily used to determine the critical collapse face pressure and its corresponding failure pattern for any tunnel model.

4. Comparison between the present limit analysis model and FE modeling

The proposed limit analysis failure mechanism gives two main outputs:

(i) The critical face pressure, i.e. the minimum required pressure to be applied to the tunnel face in order to avoid collapse.
(ii) The pattern of the most critical failure mechanism corresponding to the calculated critical collapse pressure.

Both, the critical pressure and the failure pattern should reflect the actual behavior at the tunnel face. After checking that only one critical failure mechanism exists within a multilayered soil medium, the analytical results will be compared to those obtained from 3D finite element numerical model using Midas-GTS software, a numerical model being the most reliable and comprehensive tool used in tunnel design.

In fact, although the numerical modeling by finite element/finite difference methods enables the geotechnical engineer to perform advanced numerical analyses using complex soil models, these numerical models can be highly time consuming, depending on the complexity of the problem being treated and the fineness of the mesh (especially for 3D problems as is the case in the present paper). Furthermore, these models require numerous input parameters. At an early design stage, a preliminary assessment of the tunnel stability is needed. Also, in the absence of detailed design information and/or sufficient soil data, a sensitivity analysis might be required for the evaluation of the different design scenarios. In this case, the numerical models are found to be too exhaustive, demanding (in terms of input data) and time consuming and can be replaced with more simplified analytical solutions that are equally reliable.

Face stability was extensively studied in literature using 3D numerical simulations (e.g. Al-Hallak, 1999; Anagnostou et al., 2011; Berthoz et al., 2012; Chen et al., 2013; Demagh et al., 2008; Dias, 1999; Mollon et al., 2009b, 2011c, 2013a; Vermeer

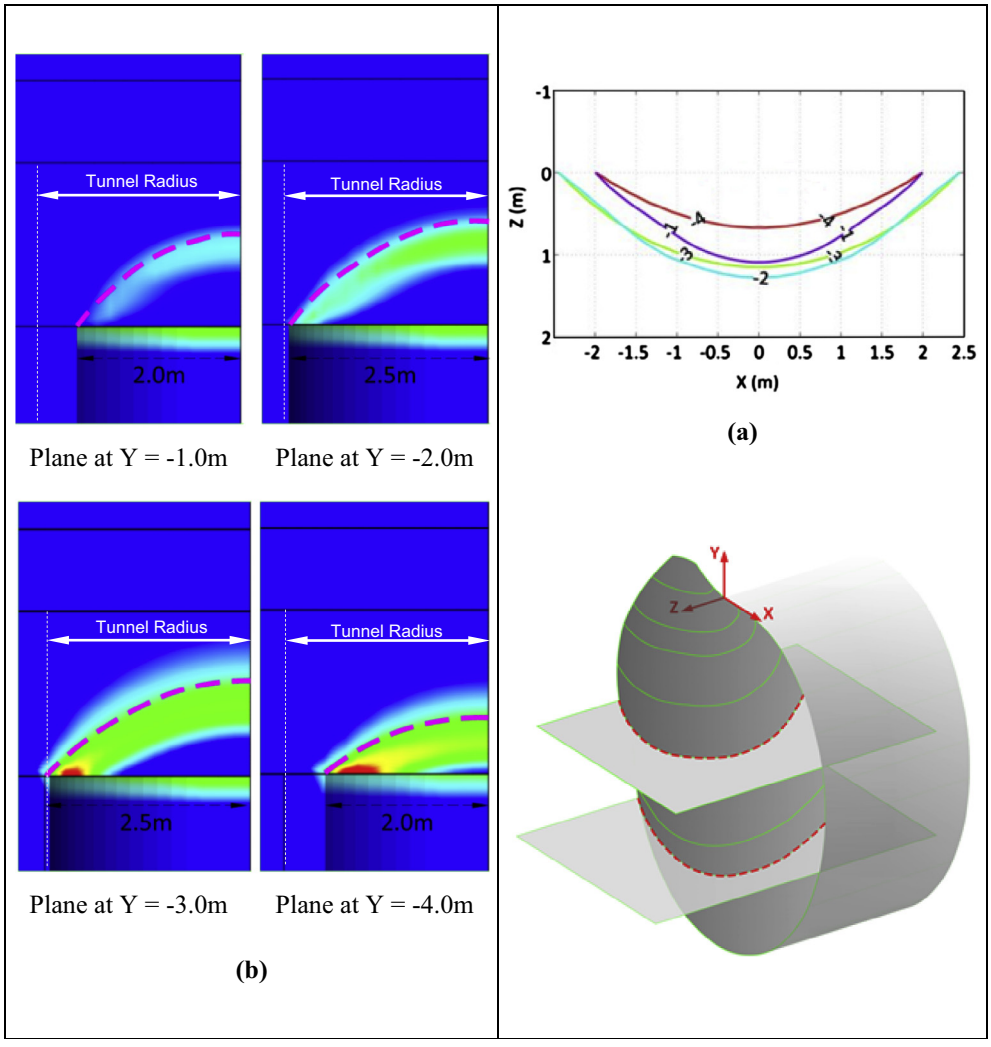

Fig. 11. Comparison between cross sections through the analytical and numerical 3D models in the planes parallel to the (*X*, *Z*) plane (at *Y* = −1.0, −2.0 m, −3.0 m and −4.0 m): (a) cross-sections through the 3D analytical failure mechanism (b) cross-sections through the 3D numerical model overlaid with the corresponding failure surface from the analytical model.

et al., 2002; Yoo and Shin, 2003). The numerical simulation results were found to give an accurate assessment of the tunnel face stability when compared to experimental results as was shown for example in Fig. 1, and as stated by several authors such as Vermeer et al. (2002), Berthoz (2012) and Chen et al. (2013).

The present limit analysis model is compared in this section to a 3D finite element model using Midas GTS software. An example of a 5.0 m tunnel diameter with a 5.0 m cover depth is considered. It is assumed that the tunnel crosses two purely frictional soil layers intersecting at the middle of the tunnel face: the upper and lower layers have friction angle values of 45° and 30° respectively. The obtained collapse pressure from the limit analysis model is of 9.1 kPa and the corresponding critical failure mechanism is shown in Fig. 7.

Concerning the numerical simulations, the model geometry is reproduced by half of the total domain due to symmetry reasons (cf. Fig. 8a). The dimensions of the model are of 7.5 m × 15 m × 12.5 m. These dimensions were proved to ensure no interaction of the displacement field with the model boundaries. Displacements are restricted at the model boundaries in the normal direction to their respective planes. The soil is assumed to be elastic perfectly plastic obeying Mohr–Coulomb yield

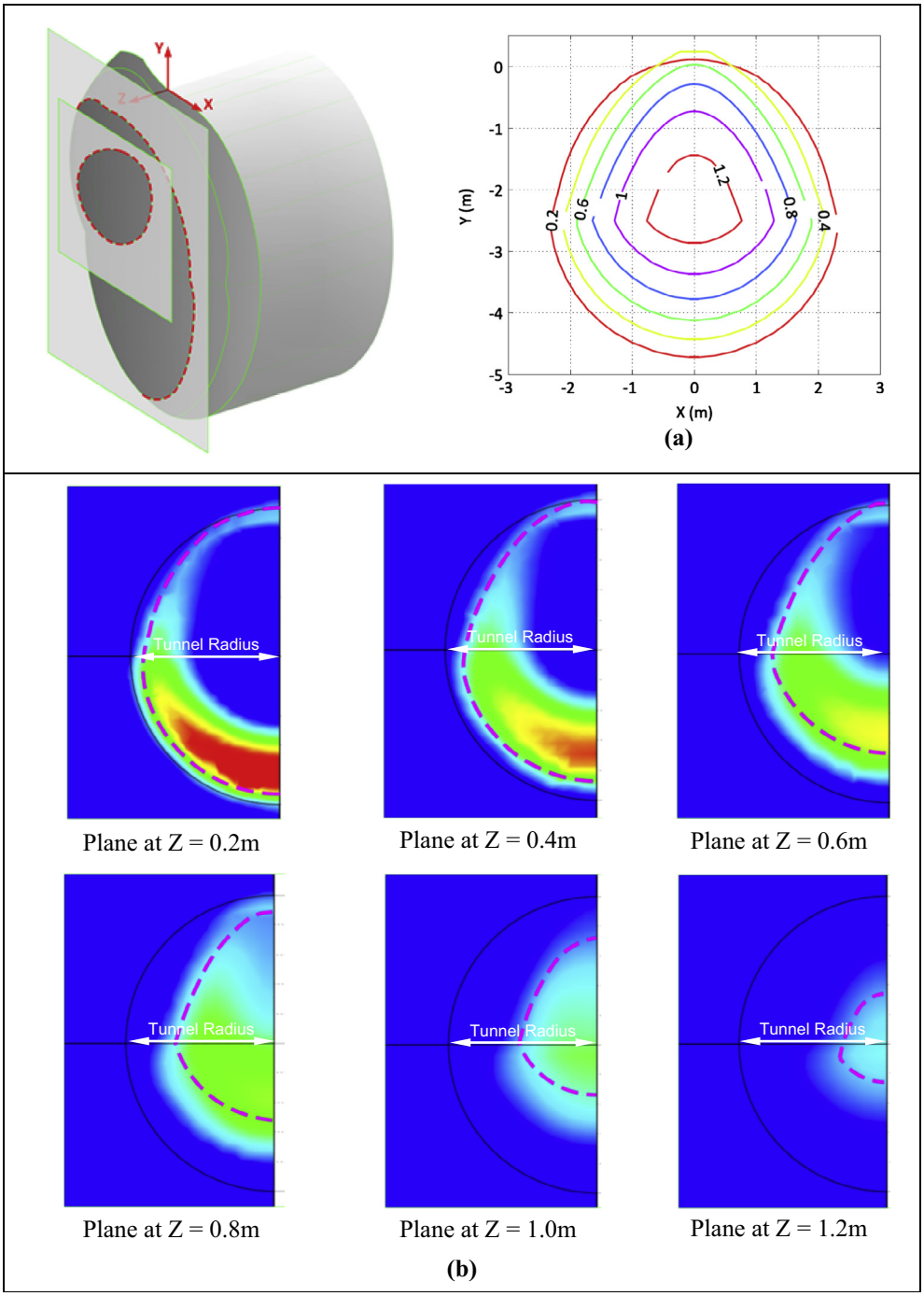

Fig. 12. Comparison between cross sections through the 3D analytical and numerical models in the planes parallel to the (*X*, *Y*) plane (at *Z* = 0.2, 0.4, 0.6, 0.8, 1 and 1.2 m): (a) cross-sections through the 3D analytical failure mechanism (b) cross-sections through the 3D numerical model overlaid with the corresponding failure surface from the analytical model (a).

criterion. The unit weight of the two soil layers is taken equal to 18 kN/m^3. Also, a Young modulus and a Poisson's ratio of 75 MPa and 0.22 respectively are adopted for the two soil layers (it has been shown by Vermeer et al. (2002) and Anagnostou et al. (2011) that these parameters have no influence on the value of the collapse pressure). Another required input parameter of the finite element model is the dilatancy angle. As stated previously, the collapse pressure obtained by limit analysis is based on an associated flow rule material ($\psi = \varphi$) in order to respect the normality condition. As the associated character of the flow rule has a limited influence on the value of the collapse pressure obtained from numerical analysis (Demagh et al., 2008; Vermeer et al., 2002), the dilatancy angles are taken here equal to the friction angles of both soil layers. The soil parameters adopted in the numerical model are given in Table 1.

The excavation process is simplified and is considered to take place in one pass. The infinite rigid lining is activated and simultaneously, a uniform face pressure is applied to the tunnel face to simulate the air pressurized shield machine. The critical face pressure is determined by successively decreasing the applied pressure until failure occurs. The collapse pressure is defined herein as the value of the applied pressure for which the software solver fails to converge (Berthoz, 2012). Besides, deformations are observed at the tunnel face for each decrement of the applied pressure. Vermeer et al. (2002) suggested that, rather than selecting a single control point at the tunnel face, it is appropriate to select a few of such points within the collapsing body, i.e. within the zone of the face that displays the maximal displacement values (cf. Fig. 8b).

4.1. Comparison of the critical face pressure

As mentioned before; in order to determine the critical face pressure by numerical simulations, the pressure applied to the tunnel face is successively decreased and the deformations are observed at the tunnel face at several control points where the highest deformations occur. However, the point at which the maximum displacement occurs (cf. Fig. 8) is adopted hereinafter as a representative control point. The pressure value for which the software solver fails to converge (which is defined herein as the

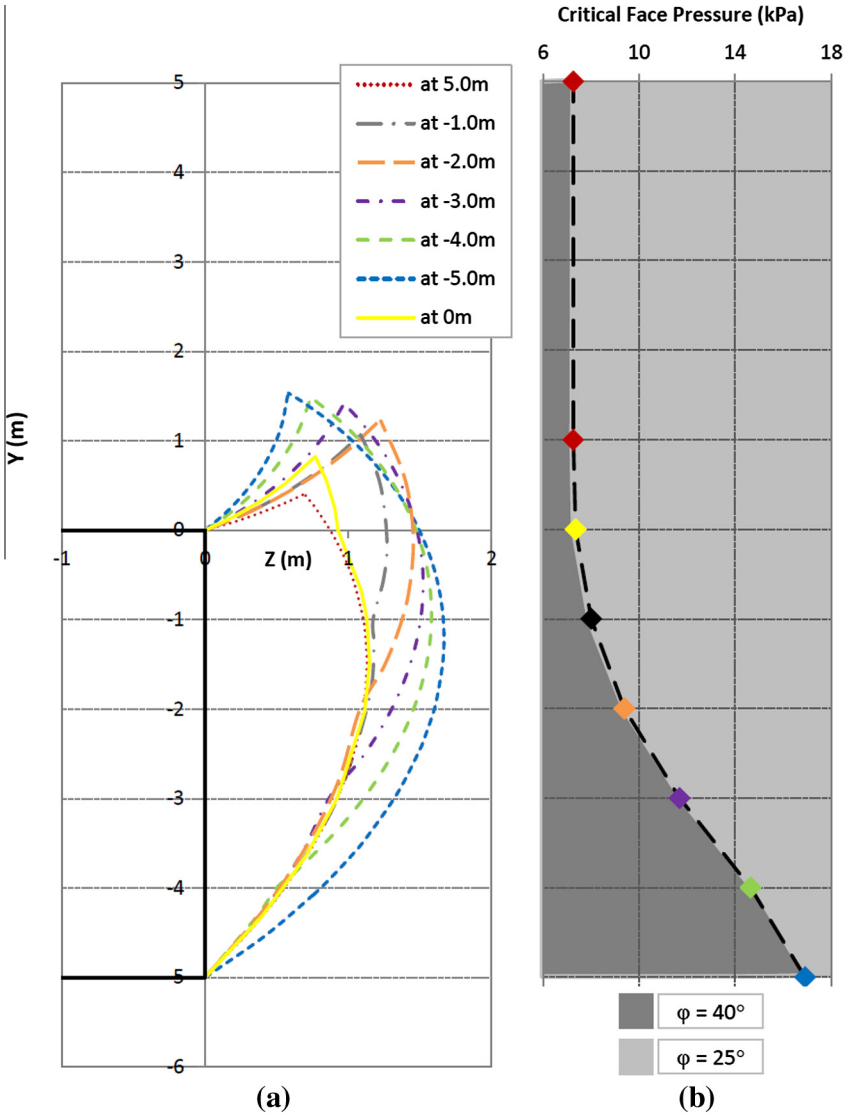

Fig. 13. Cross-sections of the critical failure mechanism for a tunnel driven within a two-layers frictional medium (with the loose sand layer overtopping the dense sand layer) for different positions of the interface between layers (a) and the corresponding values of the critical face pressure (b).

collapse pressure) is equal to 8.1 kPa. As shown in Fig. 9, prior to face collapse, deformations first follow a linear trend when plotted versus to the applied face pressure. Then, deformations deliberately increase when the face pressure becomes smaller than 8.1 kPa, indicating instability as expected for a cohesionless soil material (Anagnostou et al., 2011). When comparing the obtained collapse face pressure, the numerical model yielded an 11% lower value than the analytical model (i.e. 8.1 kPa and 9.1 kPa respectively). However, the numerical model was expected to give a higher critical face pressure than the proposed limit analysis model, as a direct consequence of the kinematic approach (as explained earlier). This anomaly was addressed by Mollon et al. (2011a–c) and was proven to be related to the mesh coarseness of the numerical model. In fact, Mollon et al. (2011a–c) found that a refinement of the mesh (up to 16 times with respect to the standard mesh) increased the critical collapse pressure to become higher than the one obtained from the limit analysis model. As the gained accuracy in the results is marginal compared to the induced increase in the needed computational time, the anomaly was deemed tolerable and the standard mesh described earlier was kept.

4.2. Comparison of the critical failure pattern

The 3D failure mechanism obtained from the limit analysis model is compared with the plastic shear strain pattern obtained by numerical simulations. Several cross-sections parallel to the (X, Y), (X, Z) and (Y, Z) planes are made through the 3D numerical model and the analytical 3D failure mechanism and are compared to each other's. For the analytical model, the slip lines delimitating the model are plotted in each direction at several offsets. As for the numerical model, Midas-GTS provides the cross-section of the plastic shear strains field on a specified plane. For every considered crossing plane, the corresponding analytical cross-section and plastic shear strains distribution are superimposed.

Figs. 10–12 show a good agreement between the resulting failure shapes. However, the boundary of the failure mass as provided by the numerical model appears to be slightly extended beyond that of the analytical model which provides a sharp and neat failure shape. This is due to the coarseness of the mesh, as was shown by Mollon et al. (2011b) who realized a similar study in 2D for a single layer with several local refinements of the mesh (up to 16 times finer than the standard mesh).

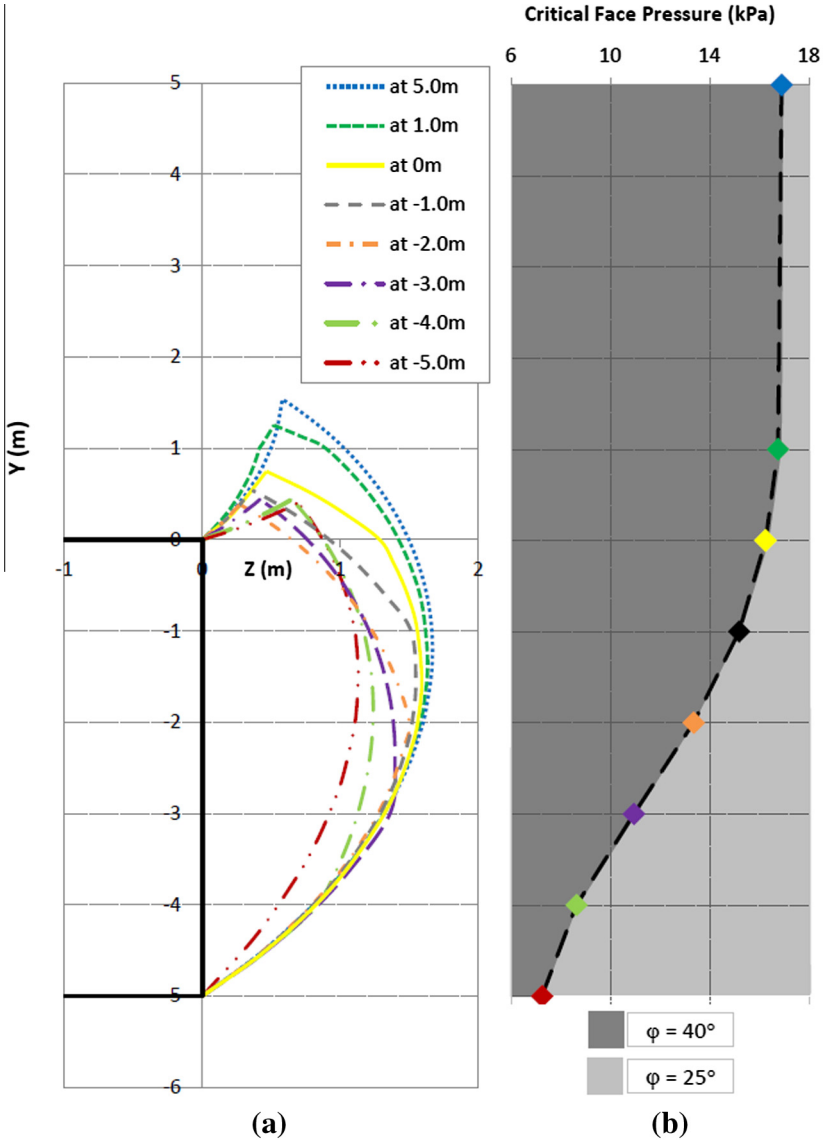

Fig. 14. Cross-sections of the critical failure mechanism for a tunnel driven within a two-layers frictional medium (with the dense sand layer overtopping the loose sand layer) for different positions of the interface between layers (a) and the corresponding values of the critical face pressure (b).

5. Application of the limit analysis model to two- or three-layers soil medium

The present 3D failure mechanism is used in this section as a practical tool to search for the critical collapse pressure and the corresponding most critical failure mechanism. In the following paragraphs, two cases of tunnels driven in two and three soil layers (with the presence of a loose layer in each case) are going to be observed, noting that, for both cases, the effect of the loose layer is emphasized.

5.1. Case of a two-layers soil medium

The example of a tunnel driven through two frictional soil layers is considered. One of the layers is composed of loose sand with $\varphi = 25°$ while the other one is a dense sand with $\varphi = 40°$. The unit weight of both soil layers is taken equal to 18 kN/m^3 The position of the interface between both layers is varied from the tunnel invert to the ground surface in order to observe its effect on the critical face pressure and the corresponding critical mechanism.

First, the layer with $\varphi = 25°$ is considered to overtop the soil layer with $\varphi = 40°$ (Fig. 13). When the thickness of the bottom layer is null (or when the interface between layers lies on the tunnel invert), the critical face pressure is equal to 16.9 kPa and it corresponds to the critical failure mechanism that could be obtained within a $\varphi = 25°$ homogeneous soil. While increasing the thickness of the bottom dense layer and thus reducing the one of the loose layer, the required critical face pressure to ensure face stability decreases and the tunnel face becomes gradually more stable. When the position of the interface between layers becomes higher than around 0.5 m of the tunnel crest, the critical face pressure becomes unchanged with a value of 7.25 kPa corresponding to the case of a homogeneous dense layer with $\varphi = 40°$.

The second configuration is the opposite of the first one because the dense sand layer is now overtopping the loose sand layer (Fig. 14). As mentioned above, when the tunnel face is driven within the dense sand, the critical face pressure is of 7.25 kPa. When the bottom loose layer is introduced, the critical face pressure progressively increases (the tunnel face becoming more unstable). The failure mechanism continues to intersect both layers

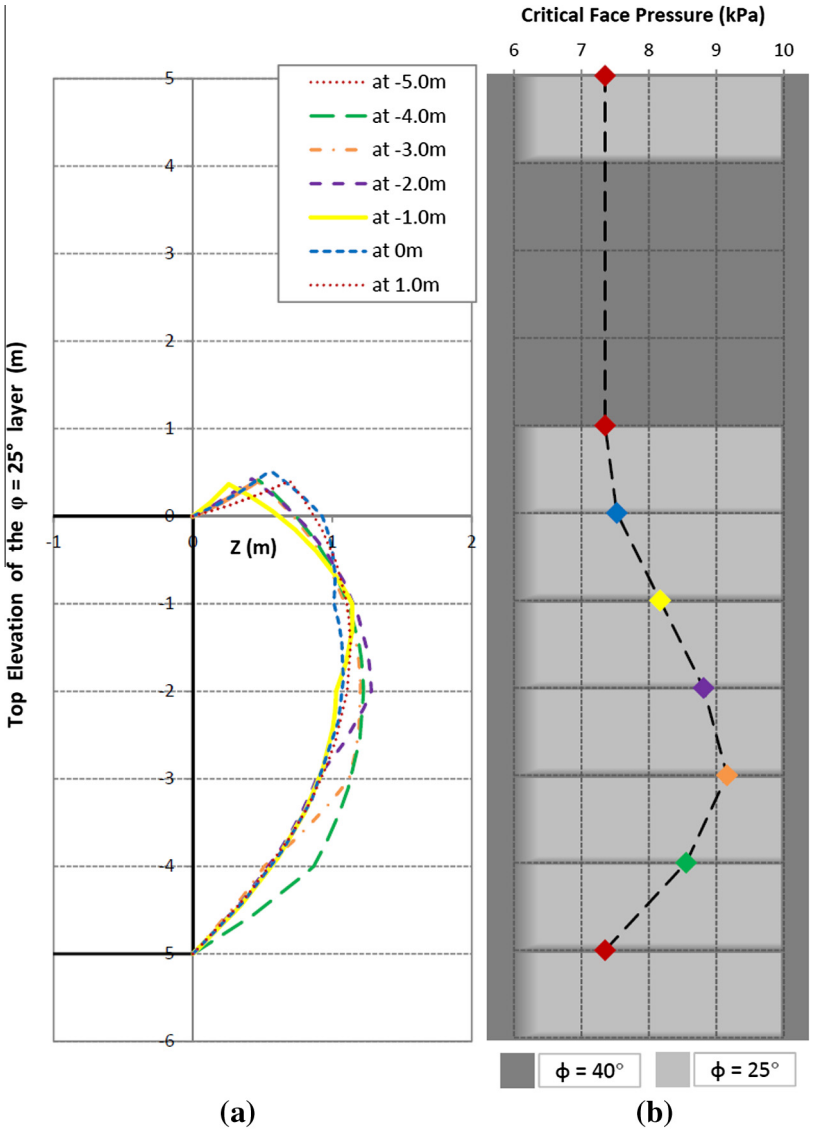

Fig. 15. Cross-sections of the critical failure mechanism for a tunnel driven within a dense sand layer intercepted by a 1.0 m thick loose sand layer for different positions of the loose sand layer (a) and the corresponding values of the critical face pressure (b).

until the top elevation of the loose layer becomes higher than 1.5 m above the tunnel crest. In this case, the failure is completely enclosed within the loose layer and the critical face pressure of 16.9 kPa is met again.

The observed limit elevation above which the most critical failure mechanism remains unchanged is related to the well-known arching effect that is taking place. Above this limit, the overtopping layer does not influence anymore the face stability. This observation is similar to the one provided by Chambon and Corté (1994). A similar result was also reported by Vermeer et al. (2002) who found that for a friction angle value higher than 20°, the ground cover and the surface loads do not influence the face stability.

5.2. Case of a three-layers soil medium

This section aims at studying the effect of the position of a loose sand layer within a dense sand layer. The example of a 5.0 m tunnel diameter driven through a dense sand layer of $\varphi = 40°$, intercepted by a 1.0 m thick loose sand layer of $\varphi = 25°$ is treated in Fig. 15. The unit weight of all soil layers is taken equal to 18 kN/m^3. The top elevation of the loose layer is varied from the tunnel invert to the ground surface in order to observe its effect on the critical face pressure and to determine the critical position for which the face stability is the most affected. As in the preceding sections, the effect of the loose layer on both the critical failure mechanism and the corresponding collapse pressure is investigated.

As shown in Fig. 15, when the top of the loose sand layer is located on the invert of the tunnel, the critical face pressure (7.25 kPa) corresponds to a single sand layer with $\varphi = 40°$. When increasing the top elevation of the loose sand layer, the critical face pressure increases which means that the tunnel face becomes less stable. The required pressure to ensure stability continues to increase until reaching a maximum at a top elevation located 3 m below the tunnel crest, corresponding to the most critical position of the loose sand layer with respect to the tunnel face. Beyond this elevation, the tunnel face pressure decreases until reaching the case of a homogeneous dense sand with $\varphi = 40°$. Interestingly, the 3D results presented here differ qualitatively from the 2D results presented in Mollon et al. (2011b). In 2D, the most critical position for a weak layer has been demonstrated to be the one at the tunnel invert, because this position is the one which maximizes the volume of the moving block. In 3D, however, the circular shape of the tunnel face leads to the fact that the lowest layer only intersects a small portion of its surface. For this reason, the most critical position for a weak layer is not the lowest one, but is located slightly higher, at about one third of the diameter.

6. Conclusion

The paper aims at presenting a 3D failure mechanism for tunnels driven under air pressurized shields within a multilayered purely frictional soil. This failure mechanism is an extension of the 3D failure mechanism developed by Mollon et al. (2011a) in the case of a single frictional layer. The results of the collapse pressures obtained from the present failure mechanism are compared with those obtained from a 3D numerical model using Midas-GTS software and they were found to be in good agreement. Also, the 3D failure pattern from the analytical model and the plastic shear strains patterns from the numerical model were superimposed through cross-sections in the 3 directions. Both failure patterns were closely matching. It should be emphasized here that it was not possible to compare the present 3D failure mechanism with the experimental results by Berthoz et al. (2012) for two and three layered soil models which consider a self-stable lower half tunnel face. Therefore, further experimental studies need to be conducted to observe the tunnel face behavior in layered soils and to validate the proposed mechanism in the case of a multilayered soil medium.

As a conclusion, the advantage of the present 3D failure mechanism over the existing analytical mechanisms is that the present mechanism can consider a multilayered medium whereas the previous ones apply only to a single soil layer which is often not the case in reality. The other advantage is with respect to the exhaustive numerical models which are much more time consuming (up to 6 h) when compared to the analytical optimization processes that requires only a few minutes computation time.

A uniform face pressure distribution was considered in this 3D limit analysis model, presuming the use of an air pressurized shield machine. This case can be further developed to cover other types of pressurized shields by adopting their relevant face pressure distribution. Furthermore, this model, considering a mechanically driven circular tunnel, can also be extended to non-circular tunnel sections excavated by conventional methods and the tunnel face stability can be assessed by computing the factor of safety (based on the strength reduction technique) instead of the critical face pressure. Moreover, the effect of the soil spatial variability on the tunnel face stability can be easily incorporated in the present mechanism (because of the mode of generation of the failure mechanism 'point by point') by considering for example the soil friction angle of each soil layer as a random field.

References

Ahmed, M., Iskander, M., 2012. Evaluation of tunnel face stability by transparent soil models. Tunn. Undergr. Space Technol. 27, 101–110.

Al Hallak, R., 1999. Etude expérimentale et numérique du renforcement du front de taille par boulonnage dans les tunnels en terrains meubles. PhD Thesis, Ecole Nationale des Ponts et Chaussées, Paris, pp. 283 (in French).

Anagnostou, G., 2012. The contribution of horizontal arching to tunnel face stability. Geotechnik 35 (1), 34–44.

Anagnostou, G., Kovari, K., 1994. The face stability of slurry-shield-driven tunnels. Tunn. Undergr. Space Technol. 9 (2), 165–174.

Anagnostou, G., Perazzelli, P., Schürch, R., 2011. Comments on "Face stability and required support pressure for TBM driven tunnels with ideal face membrane: drained case". Tunn. Undergr. Space Technol. 26, 497–500.

Berthoz, N., 2012. Modélisation physique et théorique du creusement pressurisé des tunnels en terrains meubles homogènes et stratifiés. PhD Thesis, Ecole Nationale des Travaux Publics de l'Etat, pp. 294 (in French).

Berthoz, N., Branque, D., Subrin, D., Wong, H., Humbert, E., 2012. Face failure in homogeneous and stratified soft ground: theoretical and experimental approaches on 1g EPBS reduced scale model. Tunn. Undergr. Space Technol. 30, 25–37.

Broere, W., 2001. Tunnel Face Stability & New CPT Applications. PhD Thesis, Delft University of Technology, Delft, pp. 207.

Chambon, P., Corté, J.F., 1994. Shallow tunnels in cohesionless soil: stability of tunnel face. J. Geotech. Eng. ASCE 120 (7), 1148–1165.

Chen, W.F., 1975. Limit Analysis and Soil Plasticity. Elsevier, Amsterdam.

Chen, R.-P., Li, J., Kong, L.-G., Tang, L.-J., 2013. Experimental study on face instability of shield tunnel in sand. Tunn. Undergr. Space Technol. 33, 12–21.

Demagh, R., Emeriault, F., Benmebarek, S., 2008. Analyse numérique 3D de la stabilité du front de taille d'un tunnel à faible couverture en milieu frottant. Rev. Fr. Geotech. 123, 27–35.

Dias, D., 1999. Renforcement du front de taille des tunnels par boulonnage. Etude numérique et application à un cas réel en site urbain. PhD Thesis, INSA Lyon, University of Lyon, pp. 320 (in French).

Horn, N., 1961. Horizontaler erddruck auf senkrechte abschlussflächen von tunnelröhren. Landeskonferenz der ungarischen tiefbauindustrie, 7–16.

Idinger, G., Aklik, P., Wu, W., Borja, R., 2011. Centrifuge model test on the face stability of shallow tunnel. Acta Geotech. 6, 105–117.

Kirsch, A., 2010. Experimental investigation of the face stability of shallow tunnels in sand. Acta Geotech. 5 (1), 43–62.

Leca, E., Dormieux, L., 1990. Upper and lower bound solutions for the face stability of shallow circular tunnels in frictional material. Géotechnique 40 (4), 581–606.

Meguid, M.A., Saada, O., Nunes, M.A., Mattar, J., 2008. Physical modeling of tunnels in soft ground: a review. Tunn. Undergr. Space Technol. 23, 185–198.

Mollon, G., Dias, D., Soubra, A.-H., 2009a. Probabilistic analysis and design of circular tunnels against face stability. Int. J. Geomech. Eng. 9 (6), 237–249.

Mollon, G., Dias, D., Soubra, A.-H., 2009b. Probabilistic analysis of circular tunnels in homogeneous soils using response surface methodology. J. Geotech. Geoenv. Eng. 135 (9), 1314–1325.

Mollon, G., Dias, D., Soubra, A.-H., 2010. Face stability analysis of circular tunnels driven by a pressurized shield. J. Geotech. Geoenv. Eng. 136 (1), 215–229.
Mollon, G., Dias, D., Soubra, A.-H., 2011a. Rotational failure mechanisms for the face stability analysis of tunnels driven by a pressurized shield. Int. J. Numer. Anal. Meth. Geomech. 35 (12), 1363–1388.
Mollon, G., Phoon, K.-K., Dias, D., Soubra, A.-H., 2011b. Validation of a new 2D failure mechanism for the stability analysis of a pressurized tunnel face in a spatially varying sand. J. Eng. Mech. 137 (1), 8–21.
Mollon, G., Dias, D., Soubra, A.-H., 2011c. Probabilistic analysis of pressurized tunnels against face stability using collocation-based stochastic response surface method. J. Geotech. Geoenviron. Eng. 137 (4), 385–397.
Mollon, G., Dias, D., Soubra, A.-H., 2012. Continuous velocity fields for collapse and blow-out of a pressurized tunnel face in purely cohesive soil. Int. J. Numer. Anal. Meth. Geomech. 37 (13), 2061–2083.
Mollon, G., Dias, D., Soubra, A.-H., 2013a. Probabilistic analyses of tunnelling-induced ground movements. Acta Geotech. 8 (2), 181–199.
Mollon, G., Dias, D., Soubra, A.-H., 2013b. Range of the safe retaining pressures of a pressurized tunnel face by a probabilistic approach. J. Geotech. Geoenviron. Eng. http://dx.doi.org/10.1061/(ASCE)GT.1943-5606.0000911.
Soubra, A.-H., 1999. Upper-bound solutions for bearing capacity of foundations. J. Geotech. Geoenviron. Eng. 125 (1), 59–68.
Soubra, A.H., 2002. Kinematical approach to the face stability analysis of shallow circular tunnels. In: Proceedings of the Eight International Symposium on Plasticity, Canada.
Subrin, D., Wong, H., 2002. Stabilité du front d'un tunnel en milieu frottant: un nouveau mécanisme de rupture 3D. C.R. Mécanique 330, 513–519.
Takano, D., Otani, J., Nagatani, H., Mukunoki, T., 2006. Application of X-ray CT boundary value problems in geotechnical engineering – research on tunnel face failure. In: Proc., Geocongress, ASCE, Reston, VA, pp. 1–6.
Vanoudheusden, E., 2006. Impact de la construction de tunnels urbains sur les mouvements de sol et le bâti existant – Incidence du mode de pressurisation du front. Ph.D. Thesis, INSA Lyon, University of Lyon (in French).
Vermeer, P., Ruse, N., Marcher, T., 2002. Tunnel heading stability in drained ground. Felsbau 20 (6), 8–24.
Yoo, C.S., Shin, H.K., 2003. Deformation behaviour of tunnel face reinforced with longitudinal pipes – laboratory and numerical investigation. Tunn. Undergr. Space Technol. 18 (4), 303–319.